Geophysical Research Letters

RESEARCH LETTER
10.1029/2018GL081591

Special Section:
The Three Major Hurricanes of 2017: Harvey, Irma and Maria

Persistent Hydrological Consequences of Hurricane Maria in Puerto Rico

P. W. Miller[1,2], A. Kumar[1], T. L. Mote[1], F. D. S. Moraes[1], and D. R. Mishra[1]

[1]Department of Geography, University of Georgia, Athens, GA, USA, [2]Now at Department of Oceanography and Coastal Sciences, Louisiana State University, Baton Rouge, LA, USA

Key Points:
- Landscape vegetation metrics for Puerto Rico remained depressed below pre-Maria values for approximately two months after landfall
- Cloud and precipitation activity demonstrated a stronger relationship to the atmospheric thermodynamic profile during the defoliated period
- Subsurface runoff responses to rainfall and coastal suspended sediment values remained elevated for two and four months, respectively

Correspondence to:
P. W. Miller,
pmiller1@lsu.edu

Citation:
Miller, P. W., Kumar, A., Mote, T. L., Moraes, F. D. S., & Mishra, D. R. (2019). Persistent hydrological consequences of Hurricane Maria in Puerto Rico. *Geophysical Research Letters*, *46*. https://doi.org/10.1029/2018GL081591

Received 5 DEC 2018
Accepted 23 JAN 2019
Accepted article online 28 JAN 2019

Abstract In September 2017, Hurricane Maria severely defoliated Puerto Rico's landscape, coinciding with a series of persistent hydrological consequences involving the atmospheric, terrestrial, and marine components of the water cycle. During the defoliated period, the atmosphere's thermodynamic structure more strongly explained daily cloud activity ($R^2_{PRE} = 0.02$; $R^2_{POST} = 0.40$) and precipitation ($R^2_{PRE} = 0.19$; $R^2_{POST} = 0.33$) than before landfall, indicating that post-Maria land-atmosphere interactions were comparatively muted, with similar precipitation patterns also found following Hurricanes Hugo (1989) and Georges (1998). Meanwhile, modeled post-Maria runoff exceeded statistical expectations given the magnitude of contemporaneous precipitation. Enhanced runoff also coincided with greater sediment loads in nearshore waters, increasing sediment content greater than twofold. This study offers a holistic narrative of hydrospheric disturbance and recovery, whereby the instantaneous, large-scale removal of vegetation is accompanied by hydrologic changes "upstream" in the atmosphere and "downstream" in rivers and estuaries.

Plain Language Summary Although hurricanes pose well-communicated short-term wind and storm surge threats, this study documents persistent disruptions to the regional water cycle that can last for months following landfall. When Hurricane Maria struck Puerto Rico, its strong winds removed large amounts of leaf cover from the island's forests. In the months that followed, the absence of the typical vegetation cover coincided with a stronger relationship between a tropical weather forecasting parameter and subsequent cloud and precipitation activity. Simultaneously, a greater amount of sediment was washed through streams and rivers into coastal waters. The sediment content of nearshore ocean waters remained elevated for four months following Maria's landfall. Through the modification of land-surface vegetation, hurricanes are hypothesized trigger changes to the water cycle extending to both the atmosphere as well as the stream and river networks, ultimately deteriorating coastal water quality.

1. Introduction

On 20 September 2017, Hurricane Maria (hereafter simply "Maria") made landfall on the southern coast of Puerto Rico as a powerful category-4 hurricane. With maximum sustained winds estimated at 69 m/s (155 mph), the storm devastated both the commonwealth's built and natural environments as it traversed the entire meridional width of the island (NOAA, 2017). The damage to infrastructure was staggering with 62,000 customers still lacking electrical service more than six months afterward (DOE, 2018). The true human loss will likely never be known, but excess mortality estimates include 1,085 (Santos-Lozada & Howard, 2018), 2,975 (Milken Institute School of Public Health, 2018), and 4,645 deaths (Kishore et al., 2018). Maria also decimated the island's rainforests, including the Luquillo Mountains and its fragile cloud forest (Miller et al., 2018), threatening the services they provide via drinking water and tourism, as well as their biological diversity (Quiñones et al., 2018).

Beyond its intrinsic ecological value, Puerto Rico's densely vegetated landscape also interacts with the surrounding atmosphere to influence regional weather patterns. The vegetation covering the landscape represents a store of moisture that is slowly released into the atmosphere via evapotranspiration (ET; Schellekens et al., 2000; Shukla & Mintz, 1982) moistening the boundary layer. Following the landfall of Hurricane Hugo (1989), scientists working in the Luquillo Mountains noted a three-month dry spell and a 300-m ascension of the orographic cloud base (Scatena & Larsen, 1991), positing that the changes were tied Hugo-related defoliation.

Although Hugo-era hydrological observations are limited to anecdotes, they are consistent with a theoretical link between landscape defoliation and modified cloud/precipitation patterns. When ET and its

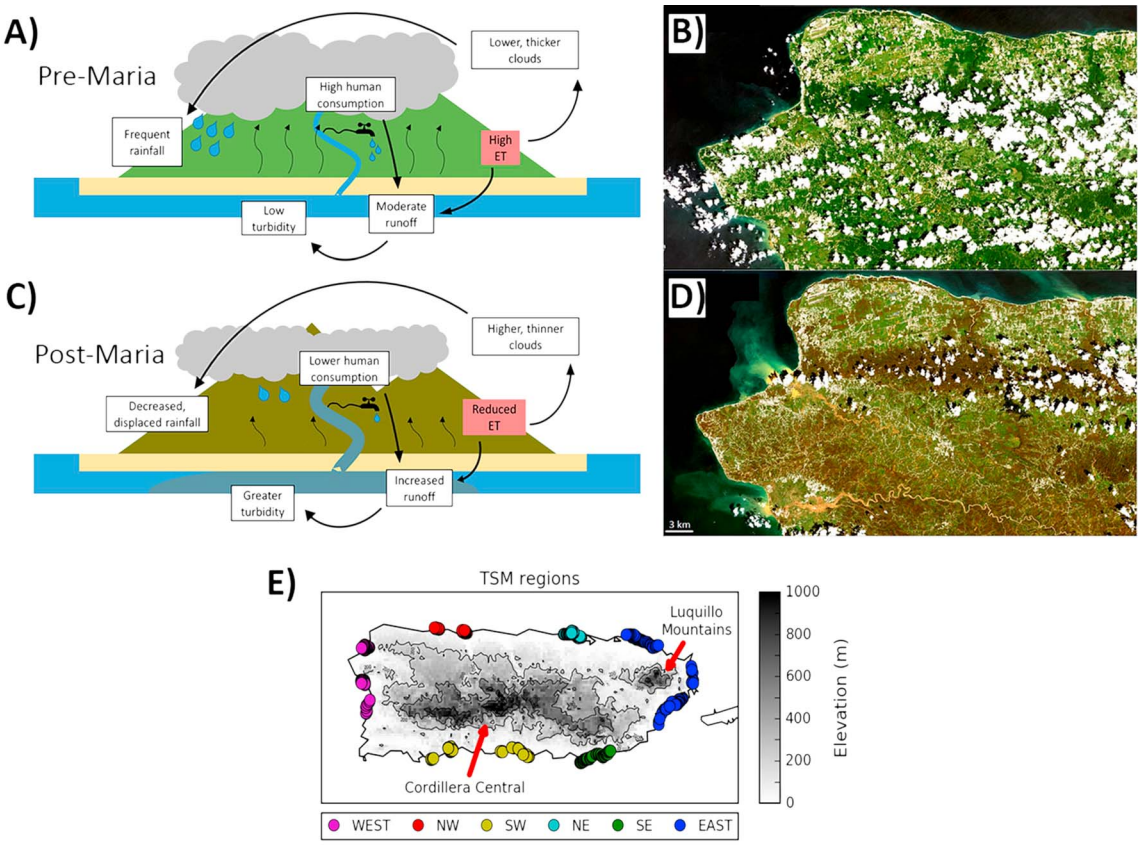

Figure 1. (a and c) Conceptual schematic of theorized hydrologic changes related to mass defoliation. (b and d) Landsat 8 Operational Land Imager (OLI) images of Northwest Puerto Rico during corresponding timeframes depicted in (a) (1 September 2017) and (c) (3 October 2017) related to Hurricane Maria. The land surface shows a visible "browning," cloud cover is reduced, rivers are turbid and swollen, and sediment plumes characterize shallow coastal waters. (e) Topographic map of Puerto Rico including the 420 pixels contributing to the coastal turbidity analysis shown as color-coded circles. The regional pixel totals are $N_{EAST} = 110$, $N_{WEST} = 110$, $N_{NE} = 50$, $N_{NW} = 50$, $N_{SE} = 50$, and $N_{SW} = 50$.

corresponding latent heat flux is reduced, heat absorbed by the landscape from incident solar radiation must be largely transferred to the atmosphere via sensible heat (i.e., increased temperature), increasing the Bowen ratio (Forrester et al., 2018). Simultaneously, satellite imagery following strong hurricanes depicts that a clear surface "browning" and modified surface reflectance in the shortwave spectrum may further alter the sensible heat flux. As near-surface temperature increases, boundary layer relative humidity would hypothetically decrease due to increased saturation vapor pressure at higher temperatures. Near-surface air parcels must then be lifted higher to adiabatically cool to saturation, retarding clouds and precipitation.

Whereas the processes above relate to the surface energy budget, the water budget is also hypothetically affected. With less foliage to intercept precipitation, throughfall, streamflow, and sediment loadings likely increase. Simultaneously, reduced ET increases surface water available for runoff, and storm-related infrastructure damage would limit human withdrawals (Quiñones et al., 2018), transmitting streamflow to ocean outlets more efficiently. Streams and rivers become swollen and muddy while their terminal estuaries experience modified salinity gradients and increased turbidity (Sommerfield et al., 2017). Figures 1a–1d illustrate these theoretical relationships conceptually and provide an anecdotal observed example following Maria.

Although these processes have been previously documented in isolation (e.g., Kumar et al., 2017; Paerl et al., 2001; Tanner et al., 1991), Maria's impact on Puerto Rico presents a unique, though unfortunate, opportunity to holistically study the hydropshere's atmospheric, terrestrial, and marine components as the land surface recovers. Thus, this paper will describe the coevolution of hydrological processes across all three components of the Puerto Rico Earth system (land, sea, and air) following Maria's mass defoliation. The objective of this paper is to identify the magnitude of these effects (if any) as well as their temporal persistence.

2. Data and Methods

Remote sensing instruments were employed to (1) characterize the magnitude of defoliation inflicted by Maria and monitor the vegetation recovery and (2) observe coincident changes to hydrological phenomena both before and after landfall. Hurricane Irma delivered a glancing blow on 7 September 2017 before Maria impacted Puerto Rico on 20 September 2017. Consequently, data were collected beginning on 1 August 2017 until 28 February 2018 to provide a one-month baseline prior to any hurricane disturbance and five whole months of posthurricane recovery.

Vegetation coverage is described using two metrics, the leaf area index (LAI) and green vegetation fraction (GVF). The LAI product (MCD15A3H), derived from the Moderate Resolution Imaging Spectroradiometer (MODIS), represents the fraction of ground area covered by one-sided green leaf material, including overlap (Myneni et al., 2015). LAI is produced directly by the MODIS science team and is available in four-day increments. For the purpose of this analysis, the radiative transfer models used to calculate the LAI are assumed to remain applicable despite the landscape disturbance. Meanwhile, the GVF calculation is a description of vegetation cover developed specifically to improve evapotranspiration schemes in numerical weather prediction models (Gutman & Ignatov, 1998). GVF, as defined by Gutman and Ignatov (1998), is derived from the normalized difference vegetation index (NDVI) using the relationship in equation (1). Essentially, the GVF attempts to contextualize each pixel's NDVI within the range of NDVIs encountered within the study domain with the lowest NDVIs expected over bare soil and the largest values over dense vegetation. The GVF was calculated according to equation (1) using MODIS daily NDVI images over Puerto Rico.

$$\mathrm{GVF} = \frac{\mathrm{NDVI} - \mathrm{NDVI}_{\text{bare soil}}}{\mathrm{NDVI}_{\text{dense vegetation}} - \mathrm{NDVI}_{\text{bare soil}}} \tag{1}$$

As shown in Figure 1d, defoliation is associated with a visible browning of the land surface, which may alter the land albedo. The daily MODIS shortwave broadband albedo product (MCD43A3) described the change in surface reflectance for the most important incoming solar wavelengths. The daily albedo product is available at 500-m resolution, and represents an estimate of the daily albedo using a 16-day retrieval window (Schaaf & Wang, 2015).

Hydrological changes in the atmosphere are characterized by the island-wide daily mean precipitation (mm) and the daily MODIS cloud-masked area (km^2). The precipitation data are retrieved from the Climate Hazard Group InfraRed Precipitation with Station, version 2.0 (CHIRPS2) data set (Funk et al., 2015). Meanwhile, cloud area was ascertained from the first 0–1 bits of the "state_1km" quality assurance band in the MODIS surface reflectance product (MOD09GA.006). The number of clouded pixels was multiplied by area of each pixel (0.5 km × 0.5 km = 0.25 km^2) to estimate the clouded area. Although ET contributes to near-surface atmospheric moisture content, cloud and precipitation processes are controlled most strongly by large-scale circulation patterns. Consequently, a pattern favoring cloud and thunderstorm activity will likely override any ET reductions from the land surface. Thus, an experimental forecasting tool, the Gálvez-Davison Index (GDI; Gálvez & Davison, 2016), is computed from radiosonde launches in San Juan, PR, to characterize the atmosphere's thermodynamic suitability to produce clouds and precipitation (Mote et al., 2017). The GDI is a unitless parameter typically ranging from −30 to 50 with larger values indicating a stronger potential for deep convection. The GDI increases as heat and humidity become concentrated in the lower levels of the atmosphere and decreases as midlevel temperatures become less favorable for convection. Radiosonde observations were retrieved from the Integrated Global Radiosonde Archive, version 2 (Durre et al., 2006).

In the soil and ocean, hydrological changes were informed using modeled subsurface runoff from the Noah land surface model within the 0.25-degree Global Land Data Assimilation System, version 2.1 (GLDAS-2.1; Beaudoing & Rodell, 2016) and total suspended matter (TSM) estimates derived from the European Space Agency's Sentinel 3-Ocean and Land Color Instrument (OLCI). GLDAS-2.1 uses observed meteorological inputs to generate storm runoff and subsurface runoff in 3-hr increments as well as monthly averages. In humid watersheds with steep slopes and permeable soils, subsurface runoff can contribute significantly to storm total runoff (Dunne, 1983; Schellekens et al., 2004), as well as represent the displacement of "old" storm water with current storm water (Pearce et al., 1986). The latter is thought to be important as reduced canopy cover will allow more water to cycle through the shallow soil layer. Although the system employs a

static vegetation classification, monthly LAI analyses are also ingested to capture any apparent changes to the land surface (Rodell et al., 2004). Thus, the GLDAS runoff values reflect the model-predicted consequences of reduced canopy interception and ET. The TSM estimates are generated using the Doerffer and Schiller (2007) algorithm which relates water-leaving radiance with absorption and backscattering coefficients via a neural network. TSM was calculated using the least clouded OLCI OL_2_WFR image for each month between August 2017 and March 2018. Near-shore waters were divided into six subregions (Figure 1e) with the sediment plumes on the 3 October 2017 post-Maria image serving as the delineation reference. All the pixels incorporated in the analysis were at least 600 m from the coast to avoid mixed-pixel contamination and benthic reflectance interference.

3. Results and Discussion

3.1. Land Cover Change and Recovery

Figure 2a shows time series of the three land surface metrics described in section 2, and depicts a clear defoliation signature following the Maria landfall. The surface albedo time series is noisy near the time of impact possibly owing to lingering Maria-related cloud cover or the reflectance of recently defoliated debris on the forest floor. Additionally, the 16-day retrieval window employed by the MODIS algorithm likely smooths any acute decreases associated with the browning in Figure 1d. Assuming that the trace is indicative of the land surface radiative properties, the time series indicates an albedo reduction of less than 10% with a quick return to pre-Maria albedo by mid-October. The marginal decrease and swift recovery suggests that either early plant regeneration promptly ameliorated the browning or that the browned surface albedo is similar to, if not slightly greater than, the dark greens typically characterizing the landscape, aligning with previous climate simulations (e.g., Bonan et al., 1992).

In contrast, the vegetation metrics paint a more coherent narrative of landscape evolution. Both the LAI and GVF show acute reductions following Maria, with the LAI also suggesting that leaf area was diminished by the passage of Hurricane Irma offshore. Hurricane Irma produced a maximum wind gust of 27.7 m/s (62.0 mph) at Luis Muñoz Marín International Airport in San Juan, PR, so impacts to the island's landscape are plausible. In the immediate aftermath of Maria, the LAI decreased from a pre-landfall mean value of 3.96 to a post-landfall mean of 0.83, a 79% reduction. Meanwhile, mean GVF values decreased from 0.60 to 0.43 during the same periods. Following the sharp reduction after landfall, both the LAI and GVF mounted a steady recovery, and returned to pre-Maria levels by late November. A regression relationship fitted to the LAI between 1 October 2017 and 1 December 2017 (equation (2); $R^2 = 0.36$, $p < 0.05$) shows that LAI recovered at an average of 0.06 units per day until returning to pre-Maria LAI levels.

$$\text{LAI} = 0.83 + 0.06(\text{days after 1 October}) \tag{2}$$

These results correspond well to other recent work characterizing Maria-related defoliation, which determined that the NDVI returned to near-normal roughly 1.5 months following landfall (Hu & Smith, 2018). In contrast, GVF showed a faster recovery compared to LAI, which could be indicative of the well-documented saturation phenomenon at low-to-moderate vegetation growth observed in NDVI-based vegetation indices (e.g., Asner et al., 2003; Sellers, 1985). The large decrease in LAI also aligns with recent studies estimating Maria-related tree mortality (Feng et al., 2018) and ecological field work performed in the immediate quiescent periods following both Hurricanes Irma and Maria (Liu et al., 2018). Using remote sensing techniques, one recent effort estimated that Maria caused immediate mortality or severe damage to 23–31 million trees (Feng et al., 2018). Similarly, forest plots sampled at four locations across Puerto Rico indicated that the pulse of litterfall associated Hurricanes Irma and Maria was equivalent to 95–171% of the mean annual total (Liu et al., 2018). However, litterfall from Hurricane Irma was actually greater than from Maria for the forest plot nearest to Irma's path, supporting the idea of an Irma-related LAI response in Figure 2a. Given the magnitude of tree mortality and defoliation, the two-month recovery window for LAI and GVF is too quick to represent a full forest recovery. Instead, field surveys in northeast Puerto Rico following Hurricane Hugo suggest that the “re-greening” was likely orchestrated by newly establishing undergrowth (Brokaw & Grear, 1991). However, it is unclear if this new foliage reproduces the ET patterns of perished mature vegetation, an important influence on hydrologic recovery.

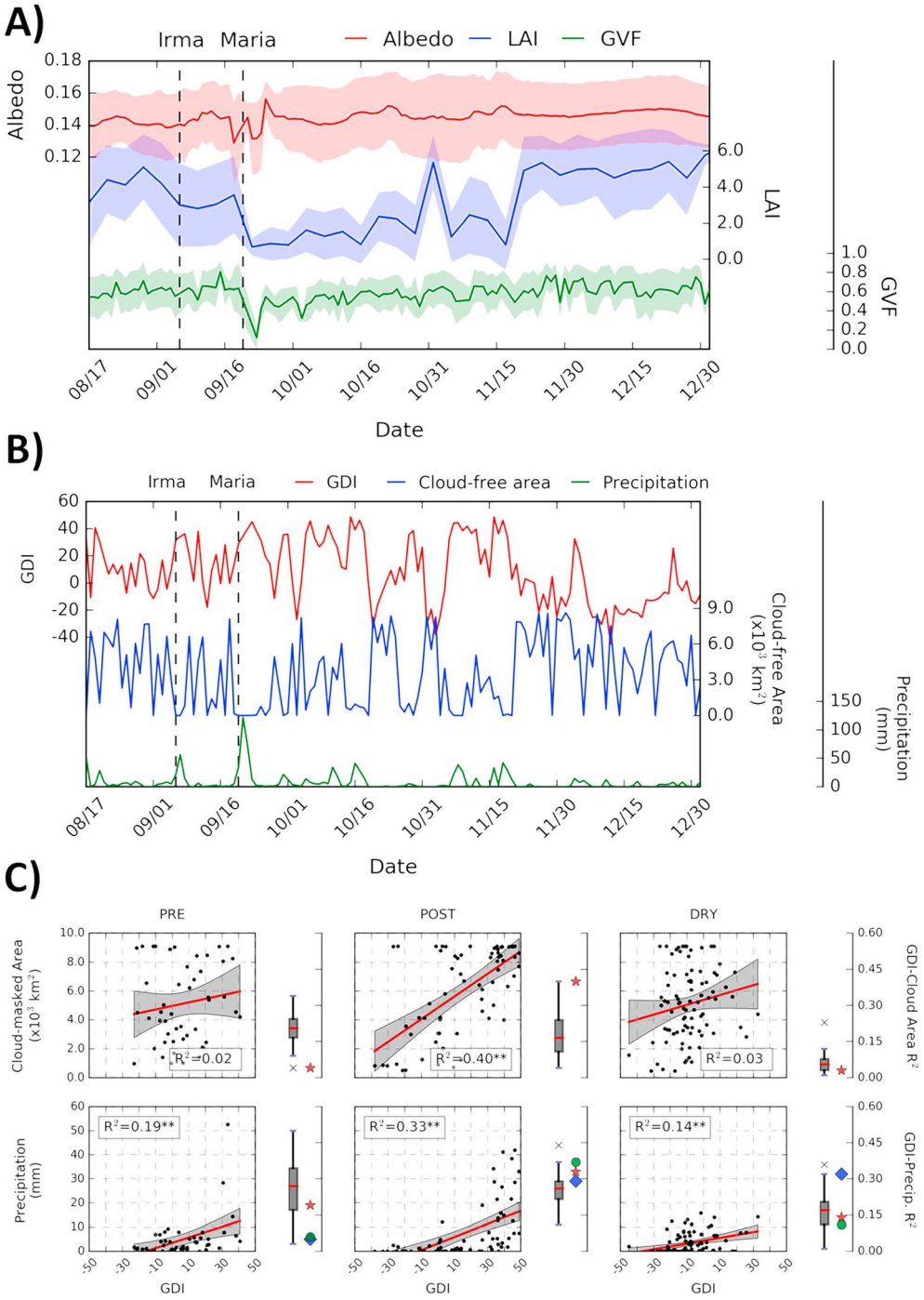

Figure 2. (a) Land cover metrics beginning roughly one month before Hurricane Maria through the end of 2017. The shaded regions bounding each trace indicate ±1σ from the mean value. (b) Time series of GDI, cloud-free area, and island-averaged precipitation. Vertical dashed lines denote the dates of Hurricanes Irma and Maria. (c) Daily MODIS cloud-mask area versus GDI segregated into three epochs: Pre-Maria ($N = 47$), post-Maria ($N = 68$), and the dry season ($N = 88$). Regression relationships for each period (red) and 95% confidence intervals (gray) for the predicted mean are denoted. Relationships significant with 95% (*) and 99% (**) confidence are denoted. For each period, box plot diagrams depict the distribution of R^2 values for the GDI-cloud area (2000–2017) and GDI-precipitation (1981–2017) relationships. The years 1989 (Hurricane Hugo), 1998 (Hurricane Georges), and 2017 (Hurricane Maria) are denoted by a green circle, blue diamond, and red star, respectively, to highlight other significant hurricane years.

3.2. Hydrological Response in the Atmosphere

Figure 2b depicts time series of daily GDI, MODIS cloud area, and island-averaged precipitation, and there is no qualitative reduction in clouds or rainfall following the landfall of Hurricane Maria. Even though diminished ET is expected to yield near-surface drying, this effect appears secondary to larger-scale atmospheric circulations as described in section 2. If the period following a defoliating event was characterized by exceptionally moist and unstable air masses, then clouds and precipitation would still occur abundantly despite diminished ET. For instance, even though mass defoliation was associated with both Hurricanes Hugo and Maria, the October–November periods following both storms were the second driest (Hugo) and fifth wettest (Maria) two-month such periods at Luis Muñoz Marín International Airport in San Juan, PR, since 1981. The mean GDI during these same two periods was 1.9 and 14.5, corresponding to the fourth lowest and fourth highest October–November averages since 1981. Consequently, any patterns in cloud cover and precipitation before and after Maria must be interpreted in the context of the thermodynamic potential to produce cloud, shower, and thunderstorm activity.

Prior to Maria, cloud cover is erratic and does not demonstrate a strong visual connection to GDI (Figure 2b). However, high post-Maria GDIs generally correspond to increased cloud cover and vice versa. Figure 2c more robustly investigates the pre-to-post Maria cloud transition. Late 2017 and early 2018 is divided into three periods: pre-Maria (1 August to 18 September 2017, excluding 6–7 September for Hurricane Irma), post-Maria (23 September to 30 November 2017), and the dry season (1 December 2017 to 28 February 2018). The post-Maria period corresponds to the span of vegetation-metric recovery, whereas they have returned to pre-Maria values during the dry season period (Figure 2a). However, as mentioned above, landscape re-greening does not necessarily signal a return to pre-Maria ET conditions. Additionally, the pre- and post-Maria periods both occur during Puerto Rico's late rainfall season (August–November; Van Beusekom et al., 2015), while 1 December marks a transition toward comparatively drier conditions annually. The GDI-cloud cover relationship shows a statistically unique transition post-Maria. Correlations are weak prior to Maria ($R^2_{CLOUD} = 0.02$, $p = 0.30$), stronger following the mass defoliation ($R^2_{CLOUD} = 0.40$, $p < 0.01$), and then weak after the vegetation metrics recover ($R^2_{CLOUD} = 0.03$, $p = 0.09$). Figure 2c also shows box plots depicting the range of annual GDI-cloud area R^2 values for the 2000–2018 August–September, October–November, and December–February periods, roughly corresponding to pre, post, and dry periods for 2017. The box plots show that the post-Maria GDI-cloud area R^2 is the strongest such relationship during the entire 18-year record.

Although the GDI-precipitation correspondence is visually less clear in Figure 2b, Figure 2c replicates the above cloud analysis for precipitation. As with the GDI-cloud relationship, correlations are weak pre-Maria ($R^2_{PRECIP} = 0.19$, $p < 0.01$), stronger following the mass defoliation ($R^2_{PRECIP} = 0.33$, $p < 0.01$), and then weak after the vegetation metrics recover ($R^2_{PRECIP} = 0.14$, $p < 0.01$). For comparison, the regression analysis is extended using the CHIRPS2 mean daily precipitation between 1981 and 2017 by calculating the distribution of GDI-precipitation R^2 values for the same annual periods as the GDI-cloud climatological analysis (1991–1992 omitted for missing radiosonde observations). The post-Maria GDI-precipitation R^2 is the fifth strongest such relationship during the 35-year archive. However, perhaps most compelling is that the 1989 (Hurricane Hugo; category 3; landfall 18 September) and 1998 (Hurricane Georges; category 3; landfall 21 September) R^2 values are also among the strongest on record (Figure 2c). Thus, each significant hurricane year in Puerto Rico ranks in the top quartile the October–November GDI-precipitation R^2 distribution, suggesting that the land-atmosphere interactions following a mass defoliation event may be systematic, not spurious.

The strengthened relationship between GDI, cloud cover, and precipitation following Maria challenged the logic stated at the outset. A drier, ET-starved boundary layer was hypothesized to disrupt the atmosphere's ability to realize its thermodynamic potential, weakening the relationship. Two possible explanations for why a defoliated landscape would promote more predictable cloud and precipitation formation are provided. (1) With a thinner tree canopy, surface roughness over the island is reduced. The prevailing northeasterly trade winds experience reduced friction as they cross the island, encountering the steep terrain with a greater velocity. Puerto Rico's orography then acts as a more effective mechanical lifting source, allowing lower tropospheric thermodynamic potential to be more readily realized. (2) Alternatively, the ET moisture input may be a source of “noise” in the atmosphere under normal conditions. ET variations may promote or

inhibit cloud and precipitation activity beyond what one would anticipate based on the GDI and the atmosphere's thermodynamic structure. Removing ET as a noise source following Maria thus strengthens the GDI-cloud and GDI-precipitation relationships. Previous work has shown orographic clouds and precipitation totals to be a function of the ambient wind speed (Colle, 2004) and moisture input from upwind land cover (Lawton et al., 2001). Unfortunately, in situ ET measurements are difficult to obtain, especially on climatological scales. However, data collected by NASA's ECOSTRESS mission, launched on 29 June 2018, will generate valuable 70-m resolution ET images that may aid similar analyses in the future.

3.3. Hydrological Response in the Rivers and Ocean

Along with influencing the above-ground hydrological cycle, sparser vegetation also poses hypothetical downstream consequences once precipitation falls to Earth. Lower interception rates allow more precipitation to reach the soil, increasing surface and subsurface runoff, streamflow, and water turbidity (Figure 1). Unfortunately, any in situ discharge measurements that survived Maria may be unreliable due to physical changes of the channel geometry that might have occurred during the hurricane. Rather than used gauged discharge measurements, changes to terrestrial hydrology are inferred using GLDAS model estimates of subsurface (Figures 3a and 3b) and storm surface (Figure 3c) runoff that incorporate monthly LAI averages into their calculations.

As Figure 2a illustrates, the LAI was severely reduced for at least six weeks following Maria's landfall, the model-predicted consequence of which is reflected in the GLDAS time series (Figure 3a). After 1 October 2017, the amplitude of modeled subsurface runoff events increases following comparable rainfall events. For instance, the island-average precipitation experienced during Hurricane Irma (6–8 September 2017) totaled 91.7 mm, and the corresponding modeled subsurface runoff response peaks at 0.75 kg/m^2 on 10 September 2017. In contrast, modified hydrologic conditions yield much different responses. Between 30 September 2017 and 6 October 2017, an island-average rainfall of 62.3 mm yields a peak modeled runoff response of 1.39 on 9 October 2017. Thus, roughly 32.1% less rainfall produced 85% greater runoff island-wide following the landscape changes resulting from Maria. Island-wide modeled subsurface runoff, which did not exceed 1.0 kg/m^2 in the month preceding Maria, breached this mark 3 times before comparatively drier conditions arrived in December.

Figures 3b and 3c contextualize the October–November 2017 modeled runoff response within the same two-month period between 2000 and 2017, the time frame that GLDAS has assimilated monthly LAI. Figure 3b shows that given the magnitude of October–November 2017 precipitation, the modeled subsurface runoff response was the most anomalous on record. Similarly, the 2017 GLDAS storm surface runoff is also significantly greater than anticipated, given the contemporaneous precipitation. Although it is tempting to ascribe the exceptional post-Maria runoff to interception impacts, surface and subsurface runoff are also controlled by antecedent soil moisture, rainfall intensity, etc., which are only coarsely resolved by the GLDAS model. Consequently, the runoff changes cannot be solely attributed to reduced interception arising from Maria's mass defoliation. For instance, the abnormal post-Maria runoff may instead be related to Maria's exceptional precipitation that saturated soils for several following weeks. Future higher-resolution hydrological modeling is needed to isolate the role of interception versus other confounding factors in yielding increased post-disturbance runoff.

The model-enhanced runoff would also presumably transport more sediment into terrestrial water channels and eventually their associated estuaries. Swollen, turbid rivers and coastal sediment plumes are still evident in Figure 1d nearly two weeks after Maria's landfall. The downstream effect on coastal water quality was monitored using remotely sensed OLCI TSM estimates from early August 2017 to early March 2018 (Figure 3d) in six different nearshore subregions. The six coastal regions are defined in Figure 1e with Figures 3e and 3f also presenting a sample comparison between a pre-Maria with post-Maria TSM image taken almost two weeks after landfall. Whereas the landscape metrics and runoff activity return to pre-Maria values by December 2017, instances of elevated nearshore turbidity persist until February 2018, more than four months after Maria's landfall.

Figure 3d shows that island-mean TSM increased 2.2 times from 5.57 mg/L two days before Maria to 12.39 mg/L two weeks after. Though rapidly declining by November, the mean TSM remains between ~5 and 6 mg/L until February 2018 when TSM decreases to 2.14 mg/L. The 2.2-times TSM increase within

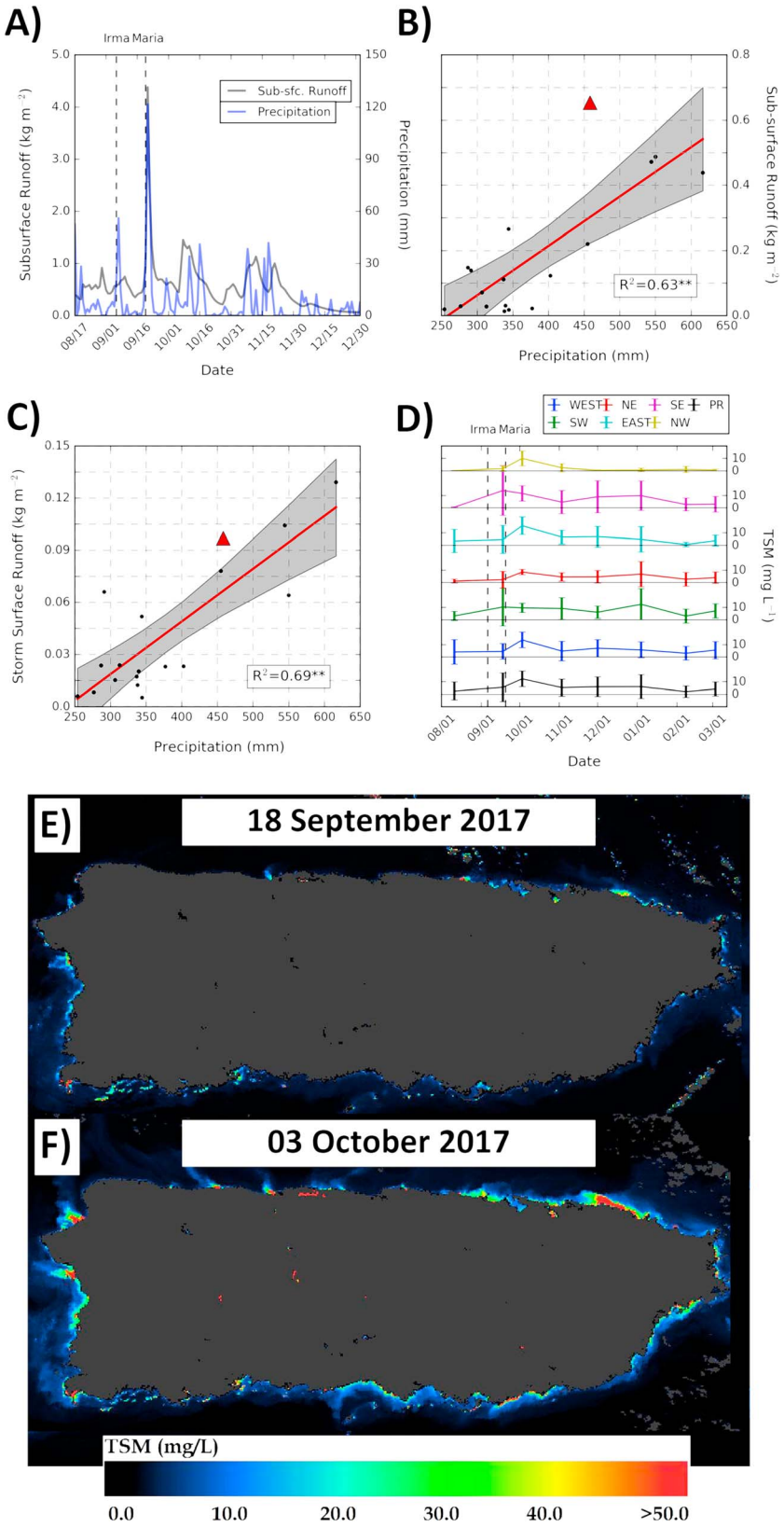

Figure 3. (a) Island-mean subsurface runoff and precipitation time series. (b) Scatterplot of island-mean subsurface runoff versus precipitation for 2000–2018. (c) Same as in (b) except for storm surface runoff. (d) Mean TSM for six subregions and their aggregation. Vertical bars indicate ±1σ from the mean. (e and f) Examples of TSM analysis.

Puerto Rico's estuaries corresponds well to previous hurricane-related sediment suspension studies. For instance, Kumar et al. (2017) found that TSM in a coastal lagoon increased ~2.5 times following the landfalls of Cyclones Hudhud (2013) and Phailin (2014) along eastern India. Similarly, Chen et al. (2009) documented TSM increases of 2.0 times during the landfall of Hurricane Frances (2004) along the U.S. Gulf Coast. However, neither study evaluated the temporal persistence of these increases. Regardless of landscape exposure, nearshore turbidity can be temporarily elevated by recent rainfall (Gellis, 2013), but directly comparing island-wide mean TSM and antecedent precipitation suggests that this cannot independently explain the TSM evolution. The 5.57-mg/L TSM on 18 September 2017 was preceded by a 14.1-mm 10-day rainfall. However, on 1 December 2017, only 5.2 mm of antecedent precipitation was associated with a 6.08-mg/L TSM. Nonetheless, these examples are anecdotal, and the defoliation contribution to enhanced TSM should be investigated through a coupled ocean-atmospheric-wave-and-sediment transport modeling system similar to Zang et al. (2018).

4. Conclusions

The catastrophic defoliation suffered during Maria is posited to have altered regional ET patterns, thereby reducing moisture emitted into the atmospheric boundary layer, increasing the surface sensible heat flux, and enhancing runoff and estuary turbidity. Following Maria, regional cloud and precipitation patterns were more strongly associated with the thermodynamic structure of the atmosphere, indicating that land-atmosphere interactions were relatively muted compared to before landfall. When precipitation did occur, modeled runoff was well above the expected magnitude based on 18 years of model output. Simultaneously, coastal sediment content increased 2.2 times after Maria, and did not return to pre-Irma values until February 2018, more than four months after Maria.

Although the hydrological changes documented here cannot be conclusively attributed to Maria's mass defoliation, they are consistent with the theoretical implications of such an event. Future modeling work is needed to isolate the defoliation's role in subsequent cloud, runoff, and TSM changes. In particular, modeling experiments may help untangle feedback loops masking the defoliation-hydrology relationship. For instance, defoliation may reduce interception and enhance surface runoff, but this effect may be offset by defoliation-related precipitation reduction.

These findings suggest that hurricane preparedness strategies should consider persistent consequences that affect a region up to four months after landfall. For instance, altered hydrological patterns may retard recovery efforts while the disaster area is particularly vulnerable. Although hurricane wind damage will acutely reduce crop and aquaculture yields, the destruction of benthic habitats via sediment smothering and the suppression of agriculture via modified rainfall may exacerbate the economic impact. These results may also adjust how local officials request disaster funding from national governments. Because officials request support promptly following the disaster, they may currently be unaware to account for persistent hydrological effects that have not yet fully manifested when soliciting funds.

Acknowledgments
This work was funded by the Georgia Sea Grant Recovery and Response to Hurricane Irma program and by the NSF Luquillo Long-Term Ecological Research Program (1239764). The authors also thank Sam Weber for the assistance with data extraction. All the derived data sets referenced in this study will be made further available at http://luq.lter.network/datacatalog upon publication.

References

Asner, G. P., Scurlock, J. M. O., & Hicke, A. J. (2003). Global synthesis of leaf area index observations: Implications for ecological and remote sensing studies. *Global Ecology and Biogeography*, *12*(3), 191–205. https://doi.org/10.1046/j.1466-822X.2003.00026.x

Beaudoing, H., & Rodell, M. (2016). GLDAS Noah land surface model L4 3 hourly 0.25 × 0.25 degree v2.1. https://doi.org/10.5067/E7TYRXPJKWOQ

Bonan, G. B., Pollard, D., & Thompson, S. L. (1992). Effects of boreal forest vegetation on global climate. *Nature*, *359*(6397), 716–718. https://doi.org/10.1038/359716a0

Brokaw, N. V. L., & Grear, J. S. (1991). Forest structure before and after hurricane Hugo at three elevations in the Luquillo Mountains, Puerto Rico. *Biotropica*, *23*(4), 386–392. https://doi.org/10.2307/2388256

Chen, S., Huang, W., Wang, H., & Li, D. (2009). Remote sensing assessment of sediment re-suspension during hurricane Frances in Apalachicola Bay, USA. *Remote Sensing of Environment*, *113*(12), 2670–2681. https://doi.org/10.1016/j.rse.2009.08.005

Colle, B. A. (2004). Sensitivity of orographic precipitation to changing ambient conditions and terrain geometries: An idealized modeling perspective. *Journal of the Atmospheric Sciences*, *61*(5), 588–606. https://doi.org/10.1175/1520-0469(2004)061<0588:SOOPTC>2.0.CO;2

DOE (2018). Hurricanes Maria & Irma April 4 event summary: Report #98. Retrieved from https://www.energy.gov/sites/prod/files/2018/04/f50/Hurricanes%20Maria%20%20Irma%20Event%20Summary%20April%204%2C%202018.pdf

Doerffer, R., & Schiller, H. (2007). The MERIS case 2 water algorithm. *International Journal of Remote Sensing*, *28*, 517–535. https://doi.org/10.1080/01431160600821127

Dunne, T. (1983). Relation of field studies and modeling in the prediction of storm runoff. *Journal of Hydrology*, *65*(1-3), 25–48. https://doi.org/10.1016/0022-1694(83)90209-3

Durre, I., Vose, R. S., & Wuertz, D. B. (2006). Overview of the integrated global radiosonde archive. *Journal of Climate*, *19*(1), 53–68. https://doi.org/10.1175/JCLI3594.1

Feng, Y., Negron-Juarez, R. I., Patricola, C. M., Collins, W. D., Uriarte, M., Hall, J. S., et al. (2018). Rapid remote sensing assessment of impacts from hurricane Maria on forests of Puerto Rico. *PeerJ Preprints*, *6*. e26597v26591. https://doi.org/10.7287/peerj.preprints.26597v1

Forrester, M. M., Maxwell, R. M., Bearup, L., & Gochis, D. (2018). Forest disturbance feedbacks from bedrock to atmosphere using coupled hydro-meteorological simulations over the Rocky Mountain headwaters. *Journal of Geophysical Research: Atmospheres*, *123*, 9026–9046. https://doi.org/10.1029/2018JD028380

Funk, C., Peterson, P., Landsfeld, M., Pedreros, D., Verdin, J., Shukla, S., et al. (2015). The climate hazards infrared precipitation with stations—A new environmental record for monitoring extremes. *Scientific Data*, *2*, 150066. https://doi.org/10.1038/sdata.2015.66

Gálvez, J. M., & Davison, M. (2016). The Gálvez-Davison Index for tropical convection. Retrieved from http://www.wpc.ncep.noaa.gov/international/gdi/GDI_Manuscript_V20161021.pdf

Gellis, A. C. (2013). Factors influencing storm-generated suspended-sediment concentrations and loads in four basins of contrasting land use, humid-tropical Puerto Rico. *Catena*, *104*, 39–57. https://doi.org/10.1016/j.catena.2012.10.018

Gutman, G., & Ignatov, A. (1998). The derivation of the green vegetation fraction from NOAA/AVHRR data for use in numerical weather prediction models. *International Journal of Remote Sensing*, *19*(8), 1533–1543. https://doi.org/10.1080/014311698215333

Hu, T., & Smith, B. R. (2018). The impact of hurricane Maria on the vegetation of Dominica and Puerto Rico using multispectral remote sensing. *Remote Sensing*, *10*(6), 827. https://doi.org/10.3390/rs10060827

Kishore, N., Marqués, D., Mahmud, A., Kiang, M. V., Rodriguez, I., Fuller, A., et al. (2018). Mortality in Puerto Rico after hurricane Maria. *New England Journal of Medicine*, *379*, 162–170. https://doi.org/10.1056/NEJMsa1803972

Kumar, A., Mishra, D. R., Equeenuddin, S. M., Cho, H. J., & Rastogi, G. (2017). Differential impact of anniversary-severe cyclones on the water quality of a tropical coastal lagoon. *Estuaries and Coasts*, *40*, 317–342. https://doi.org/10.1007/s12237-016-0172-3

Lawton, R. O., Nair, U. S., Pielke, R. A., & Welch, R. M. (2001). Climatic impact of tropical lowland deforestation on nearby montane cloud forests. *Science*, *294*(5542), 584–587. https://doi.org/10.1126/science.1062459

Liu, X., Zeng, X., Zou, X., González, G., Wang, C., & Yang, S. (2018). Litterfall production prior to and during hurricanes Irma and Maria in four Puerto Rican forests. *Forests*, *9*(6), 367. https://doi.org/10.3390/f9060367

Milken Institute School of Public Health (2018). Ascertainment of the Estimated Excess Mortality from Hurricane Maria in Puerto Rico. Washington, DC. Retrieved from https://publichealth.gwu.edu/sites/default/files/downloads/projects/PRstudy/Acertainment%20of%20the%20Estimated%20Excess%20Mortality%20from%20Hurricane%20Maria%20in%20Puerto%20Rico.pdf

Miller, P. W., Mote, T. L., Ramseyer, C. A., Van Beusekom, A. E., Scholl, M. A., & González, G. (2018). A 42 year inference of cloud base height trends in the Luquillo Mountains of northeastern Puerto Rico. *Climate Research*, *76*, 87–94. https://doi.org/10.3354/cr01529

Mote, T. L., Ramseyer, C. A., & Miller, P. W. (2017). The Saharan air layer as an early rainfall season suppressant in the eastern Caribbean: The 2015 Puerto Rico drought. *Journal of Geophysical Research: Atmospheres*, *122*, 10,966–10,982. https://doi.org/10.1002/2017JD026911

Myneni, R., Knyazikhin, Y., & Park, T. (2015). MCD15A3H MODIS/Terra+Aqua Leaf Area Index/FPAR 4-day L4 Global 500 m SIN Grid V006. https://doi.org/10.5067/MODIS/MCD15A3H.006

NOAA (2017). Tropical cyclone report: Hurricane Maria (AL152017). Miami, FL. Retrieved from https://www.nhc.noaa.gov/data/tcr/AL152017_Maria.pdf

Paerl, H. W., Bales, J. D., Ausley, L. W., Buzzelli, C. P., Crowder, L. B., Eby, L. A., et al. (2001). Ecosystem impacts of three sequential hurricanes (Dennis, Floyd, and Irene) on the United States' largest lagoonal estuary, Pamlico sound, NC. *Proceedings of the National Academy of Sciences*, *98*(10), 5655–5660. https://doi.org/10.1073/pnas.101097398

Pearce, A. J., Stewart, M. K., & Sklash, M. G. (1986). Storm runoff generation in humid headwater catchments: 1. Where does the water come from? *Water Resources Research*, *22*(8), 1263–1272. https://doi.org/10.1029/WR022i008p01263

Quiñones, M., Parés-Ramos, I. K., Gould, W. A., Gonzalez, G., McGinley, K., & Ríos, P. (2018). El Yunque National Forest Atlas. Río Piedras, Puerto Rico. Retrieved from https://data.fs.usda.gov/research/pubs/iitf/iitf_gtr_47_eng_highres.pdf

Rodell, M., Houser, P. R., Jambor, U., Gottschalck, J., Mitchell, K., Meng, C. J., et al. (2004). The global land data assimilation system. *Bulletin of the American Meteorological Society*, *85*, 381–394. https://doi.org/10.1175/BAMS-85-3-381

Santos-Lozada, A. R., & Howard, J. T. (2018). Use of death counts from vital statistics to calculate excess deaths in Puerto Rico following hurricane Maria. *JAMA*, *320*, 1491–1493. https://doi.org/10.1001/jama.2018.10929

Scatena, F. N., & Larsen, M. C. (1991). Physical aspects of hurricane Hugo in Puerto Rico. *Biotropica*, *23*, 317–323. https://doi.org/10.2307/2388247

Schaaf, C., & Wang, Z. (2015). *MCD43A3 MODIS/Terra+Aqua BRDF/Albedo Daily L3 Global - 500m V006*. https://doi.org/10.5067/MODIS/MCD43A3.006.

Schellekens, J., Bruijnzeel, L. A., Scatena, F. N., Bink, N. J., & Holwerda, F. (2000). Evaporation from a tropical rain forest, Luquillo experimental Forest, eastern Puerto Rico. *Water Resources Research*, *36*(8), 2183–2196. https://doi.org/10.1029/2000WR900074

Schellekens, J., Scatena, F. N., Bruijnzeel, L. A., Dijk, A. I. J. M. V., Groen, M. M. A., & Hogezand, R. J. P. V. (2004). Stormflow generation in a small rainforest catchment in the Luquillo experimental Forest, Puerto Rico. *Hydrological Processes*, *18*(3), 505–530. https://doi.org/10.1002/hyp.1335

Sellers, P. J. (1985). Canopy reflectance, photosynthesis and transpiration. *International Journal of Remote Sensing*, *6*(8), 1335–1372. https://doi.org/10.1080/01431168508948283

Shukla, J., & Mintz, Y. (1982). Influence of land-surface evapotranspiration on the Earth's climate. *Science*, *215*(4539), 1498–1501. https://doi.org/10.1126/science.215.4539.1498

Sommerfield, C. K., Duval, D. I., & Chant, R. J. (2017). Estuarine sedimentary response to Atlantic tropical cyclones. *Marine Geology*, *391*, 65–75. https://doi.org/10.1016/j.margeo.2017.07.015

Tanner, E. V. J., Kapos, V., & Healey, J. R. (1991). Hurricane effects on forest ecosystems in the Caribbean. *Biotropica*, *23*(4), 513–521. https://doi.org/10.2307/2388274

Van Beusekom, A. E., González, G., & Rivera, M. M. (2015). Short-term precipitation and temperature trends along an elevation gradient in northeastern Puerto Rico. *Earth Interactions*, *19*, 1–33. https://doi.org/10.1175/EI-D-14-0023.1

Zang, Z., Xue, Z. G., Bao, S., Chen, Q., Walker, N. D., Haag, A. S., et al. (2018). Numerical study of sediment dynamics during hurricane Gustav. *Ocean Modelling*, *126*, 29–42. https://doi.org/10.1016/j.ocemod.2018.04.002